Synthesis and photocatalytic performance of $SnZn(OH)_6$ with different morphologies

Wenyan Wang, Zhanwei Ma, Runjuan Liang, Tinghua Wu,[a] and Ying Wu[b]
Key Laboratory of the Ministry of Education for Advanced Catalysis Materials, Institute of Physical Chemistry, Zhejiang Normal University, Jinhua 321004, China

(Received 16 January 2013; accepted 2 May 2013)

$SnZn(OH)_6$ (ZHS) with different morphologies were synthesized by a facile self-templated method at room temperature. It was found that the morphology of ZHS could be controlled by varying the concentration of OH^-. The crystalline structure and morphology of the particles were characterized by x-ray diffraction, UV-vis diffuse reflectance spectroscopy, scanning electron microscopy images, and N_2 adsorption. The results indicated that the particles had almost uniform monoclinic geometry and uniform size. The photocatalytic activity of ZHS with different morphologies was tested through degradation of Rhodamine B (RhB). Therein, the hollow ZHS showed the highest light catalytic performance due to its large BET surface area, wide band gap, and high crystallinity.

I. INTRODUCTION

In recent years, hollow micro-/nanostructural materials have received considerable attention because of their widespread potential applications in the fields of catalysis, sensors, drug delivery, photonic crystals, rechargeable batteries, chemical reactors, and so on.[1–6]

$ZnSn(OH)_6$ (ZHS) is a kind of typical perovskite-structured hydroxide materials.[7] In the compound, the metal atoms are octahedrally coordinated with oxygen atoms to form $Sn(OH)_6$ and $Zn(OH)_6$ polyhedra, which share their "O" corners to build the structural framework.[8] ZHS has shown extraordinary performance as flame-, smoke-, and toxic gas-retardant.[9] It is mainly used as a kind of novel, nontoxic flame-retardant and environment-friendly polymeric materials.[10–12] The thermal decomposition products of ZHS, such as amorphous $ZnSnO_3$, crystalline SnO_2, and Zn_2SnO_4 also have important applications in gas sensors and Li-ion batteries.[13–15] In addition, ZHS was reported to exhibit high and stable photocatalytic activity for benzene degradation.[16] Several methods have been developed to prepare ZHS, including solid-state metathesis approaches, solvothermal reactions, hydrothermal (HT) reactions and wet sonochemical methods.[7,17,18] Recently, ZHS prepared by a solvothermal method has been reported.[16] The synthesized ZHS showed high photocatalytic activity for degradation of benzene under UV light irradiation. In general, the properties of inorganic materials are correlated with their morphology.[19] The ZHS prepared via different methods would exhibit different photocatalytic activity. For example, Chen et al. synthesized the ZHS by two facial and green methods, i.e., homogeneous precipitation (HP) and HT. The photodegradation efficiency of ZHS-HP was found to be higher than that of ZHS-HT.[20] This phenomenon inspired scientist's interest to prepare ZHS with different morphologies. Fan et al.[21] prepared ZHS hollow core–shell microspheres and polyhedral microcrystals using HT method. Qin et al.[22] synthesized single crystalline $ZnSn(OH)_6$ nanocubes on α-{Cu,Sn} copper foils by a low-temperature HT method. Wang et al.[23] synthesized single-crystalline $ZnSn(OH)_6$ hollow cubes via self-templated synthesis at room temperature, which exhibited certain photocatalytic activity for the degradation of phenol under UV light irradiation. Though ZHS has been obtained by the above methods, it is seldom reported on using a simple method to yield different morphologies of ZHS.

In this paper, single-crystalline ZHS particles with different morphologies were synthesized by an alkali-assisted dissolution process at room temperature. The photocatalytic activity of the samples was also evaluated by degradating RhB in aqueous solution.

II. EXPERIMENTAL

A. Materials and reagents

Tin (IV) chloride pentahydrate ($SnCl_4{\cdot}5H_2O$, ≥99.9%), zinc (II) chloride ($ZnCl_2$, 100%), citric acid monohydrate ($C_6H_8O_7{\cdot}H_2O$, ≥99.5%), and sodium hydroxide (NaOH, ≥98.0%) were purchased from Aladdin Chemistry Co. Ltd. (Shanghai, China). All reagents were of analytical grade and used without further purification.

B. Preparation

A typical synthesis of ZHS cubes by co-precipitation method is as follows: 0.137 g $ZnCl_2$ and 0.21 g $C_6H_8O_7{\cdot}H_2O$

Address all correspondence to these authors.
[a]e-mail: thwu@zjnu.cn
[b]e-mail: yingwu@zjnu.cn
DOI: 10.1557/jmr.2013.147

 © Materials Research Society 2013

https://doi.org/10.1557/jmr.2013.147 Published online by Cambridge University Press

were first dissolved in 10 mL of distilled water. Simultaneously, 0.351 g $SnCl_4 \cdot 5H_2O$ was dissolved in 5 mL of anhydrous ethanol. The Sn^{4+} solution was dropped into the Zn^{2+} solution to obtain a mixed solution. Then, NaOH solid was directly added to obtain a white precipitate.[24] After stirring at room temperature for 10 min, 25 mL of distilled water was also added. The whole process was conducted in a magnetic stirring apparatus. These white precipitates were centrifuged and rinsed thoroughly with distilled water and anhydrous ethanol several times, and finally dried at 60 °C for 10 h. The precipitate was obtained by adding 0.409, 0.613, and 0.818 g NaOH solid were denoted as S1, S2, and S3, respectively. Besides, a part of S1 was also subjected to adding 20 mL of 2 M NaOH solution dropwise into the precursor solution. The obtained sample was denoted as S4.

C. Characterization

X-ray diffraction (XRD) patterns of the catalysts were obtained on a Philips x-ray diffractometer (PW 3040/60, Amsterdam, Netherlands) using Cu K_α radiation. The accelerating voltage and the current were 40 kV and 40 mA, respectively. The scanning electron microscopy (SEM) images were taken on a field emission scanning electron microscope (Hitachi S-4800, Tokyo, Japan). UV-vis diffuse reflectance spectrum (UV-vis DRS) was recorded in the range of 200–800 nm on a UV-vis spectrometer (Nicolet, evolution 500, Thermo, MA), where $BaSO_4$ was used as a reference sample. Pore structure parameters of the samples, including Brauner–Emmett–Teller (BET) surface areas and density-functional-theory pore size distribution, were determined according to the nitrogen adsorption–desorption isotherms measured at 77 K using a physisorption apparatus (Quantachrome Autosorb-1, Boynton Beach, FL).

D. Catalytic performances

The catalytic activity was measured by a self-made photoreaction apparatus. A 500 W Hg lamp was used as a source of UV light. The dominant wave length was 284 nm. The photocatalytic activity of ZHS was evaluated by the degradation of RhB. The initial concentration of RhB is 1.0×10^{-4} mol/L, and the concentration of ZHS is 0.5 g/L. To disperse the catalyst powder and reach the adsorption–desorption equilibrium on the photocatalyst surface, the suspensions were stirred for 1 h in the dark before irradiation. During the RhB photodecomposition, the samples were withdrawn at regular intervals and centrifuged by a low speed centrifuge. The absorption of filtrate was measured in the range of 450–600 nm by using a UV-vis spectrophotometer (TU-1810, Beijing, China).

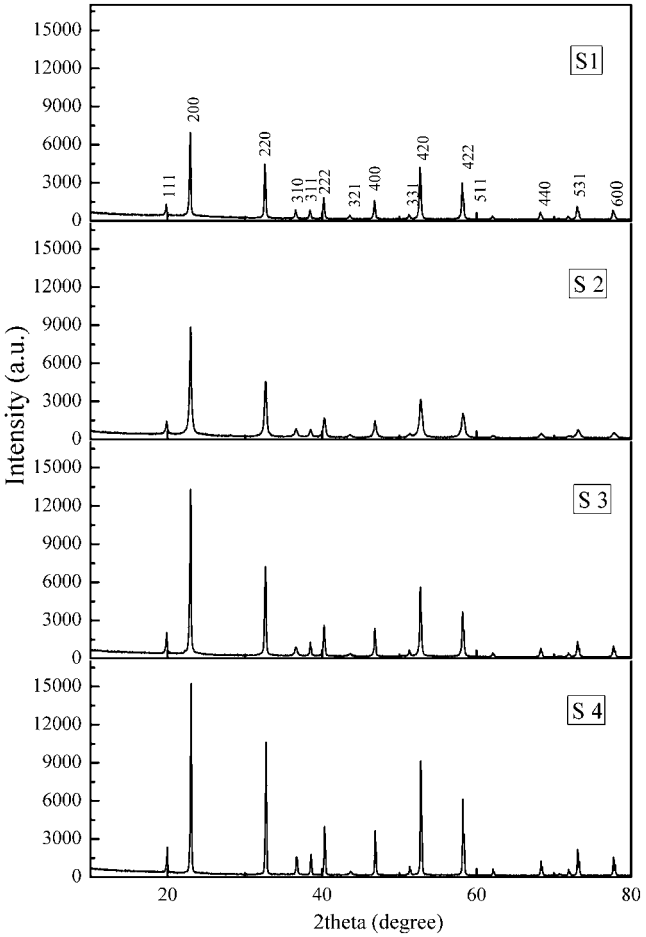


FIG. 1. XRD pattern of the as-prepared ZHS via adding different amounts of NaOH (S1, S2, S3, and S4).

III. RESULTS AND DISCUSSION

A. Structure and phase

The phase purity of the as-prepared ZHS samples was obtained by XRD and the results are shown in Fig. 1. The peaks in the XRD patterns match the $SnZn(OH)_6$ (JCPDS No. 20–1455). No additional peaks of other impurities were observed, indicating that the as-prepared samples are pure ZHS. S3 and S4 samples exhibit sharp and strong peaks, which might be ascribed to their high crystallinity.[25] To prove the deduction above, the peak ($2\theta = 22.7°$) area was calculated by Gauss fitting. The result shows that the peak areas for S1, S2, S3, and S4 are 1441, 2627, 2695, and 2831, respectively. If the sample (S4) which has the largest peak area was selected as a standard, the calculated crystallinity of other three samples would be 50.9% (S1), 92.8% (S2), and 95.2% (S3), respectively. It is definite that the crystallinity of the samples decreases in the order of S4 > S3 > S2 > S1. In addition, the average particle size of four particles was calculated using the Debye–Scherrer formula, $D_{hkl} = K\lambda/\beta\cos\theta$, where λ is wave length of the Cu K_α used, β is the full

https://doi.org/10.1557/jmr.2013.147 Published online by Cambridge University Press

width at half maximum of the diffraction angle considered, K is a shape factor (0.94), and θ is the angle of diffraction.[26] The particle sizes of the four samples were S1 = 37 nm, S2 = 24 nm, S3 = 38 nm, and S4 = 44 nm, respectively.

B. Morphology evolution

Figure 2 shows the SEM images of as-prepared ZHS samples. It is clear that the amount of added NaOH affects the morphologies of ZHS. When the amount of NaOH solid was 0.409 g, cubes ZHS-S1 can be obtained, as shown in Fig. 2(a). When the amount of NaOH was increased to 0.613 g, we got spheres ZHS-S2 [Fig. 2(b)]. A higher amount of NaOH (0.818 g) would result in polyhedron (tetrakaidecahedrons) ZHS-S3 [Fig. 2(c)]. From the SEM images (S1, S2, and S3), it also can be observed that with the increased amount of solid NaOH in the first step, not only the morphologies changed, but also the particle sizes became nonuniform (see Figs. S1 and S2).

The hollow cubes can be obtained by one additional step. Figure 2(d) shows that the synthesized hollow cubes are of uniform size with an average edge length of 600–800 nm. The hollow cubes contain sharp corners and some cubes exhibit holes in the corners [Fig. 2(e)], indicating that the particles have a hollow interior. The thickness of the cell wall is about 50–100 nm. With the increase of the volume of 2 M NaOH solution, the cell wall of the hollow cubes will become thinner and the holes in the corners also become bigger [Fig. 2(f)].[23]

Owing to only the change in concentration of OH^- during the preparation process, it indicated that the morphologies of ZHS strongly depend on the amount of OH^-. Changing the pH of the reaction system can control the total surface

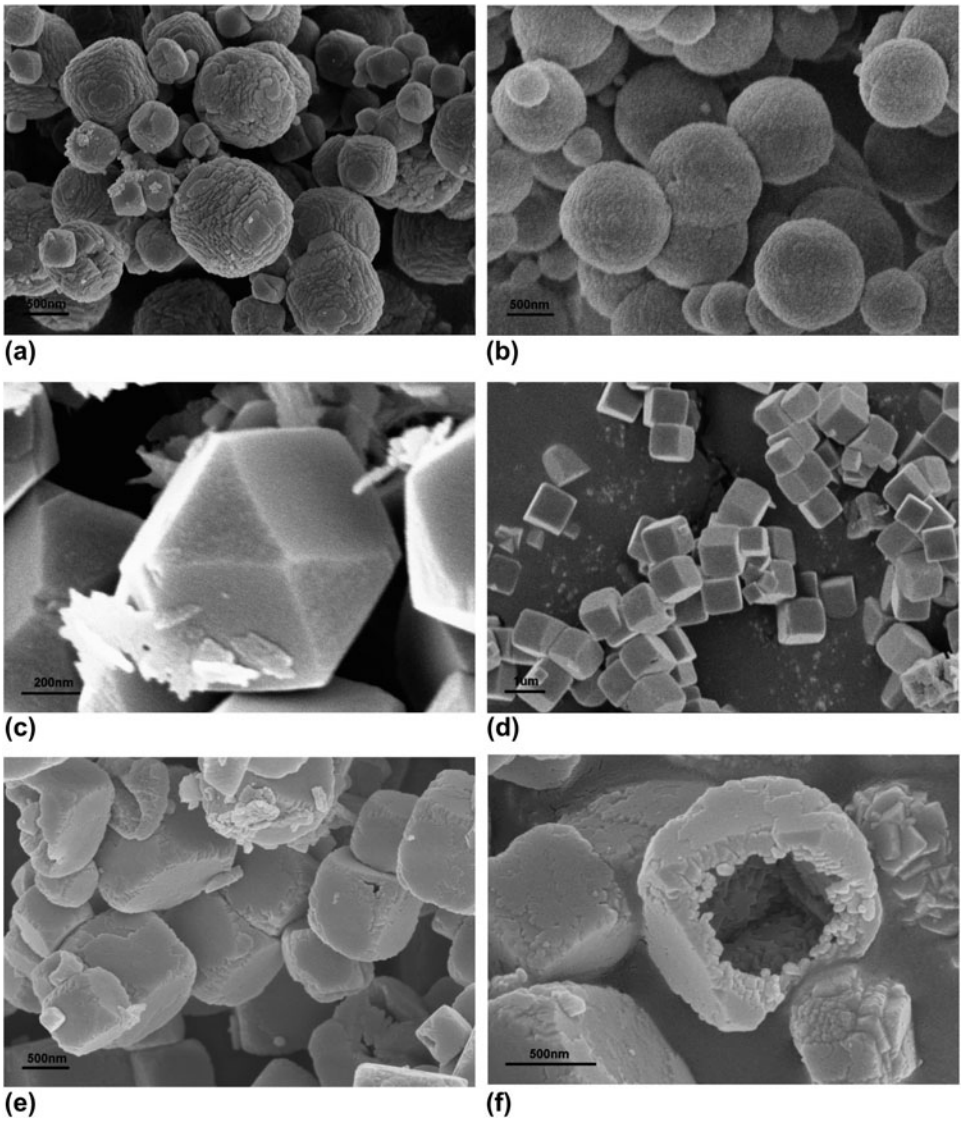


FIG. 2. SEM images of the as-prepared samples via adding different amounts of solid NaOH. (a) S1, (b) S2, (c) S3, and (d), (e), and (f) S4.

https://doi.org/10.1557/jmr.2013.147 Published online by Cambridge University Press

energy of the system and conduct the growth of the crystal. In this experiment, with the concentration of OH^- increasing, the H^+ was gradually neutralized. The concentration of H^+ on the surface of ZHS would be changed, which resulted in a significant difference in the surface free energy in each crystal surface. Some crystal surfaces with higher surface free energy grow faster than those with lower surface free energy.[27,28] ZHS is one of the perovskite oxides with face-centered-cubic close-packing. The face-centered-cubic crystal has a general sequence of surface energies, $\gamma\{111\} < \gamma\{100\} < \gamma\{110\}$. The crystals would be enclosed with {111} planes as the basal surfaces to minimize surface energy, while {100} or {110} lattice planes with relatively high surface energies might grow faster and ultimately disappear during the crystal growth.[29,30] The anisotropic growth of the crystal would make the ZHS present different morphologies, such as cube, sphere, and polyhedron. For hollow cubes (S4), Wang et al. have reported that hollow cubes are formed in a two-step process. The solid cubes were prepared from a rapid co-precipitation in the first step, followed by a self-templated transformation of the solid to hollow cubes through an alkali-assisted dissolution in the second step. The main reactions in the two steps are listed as follows:

$$Zn(II)(aq) + Sn(IV)(aq) + 6OH^-(aq) \rightarrow ZnSn(OH)_6 \quad , \tag{1}$$

$$ZnSn(OH)_6 + 4OH^-(aq) \rightarrow Zn(OH)_4^{2-} + Sn(OH)_6^{2-} \quad . \tag{2}$$

The surface free energy of edge and corner sites is relatively higher in thermodynamics.[17] Therefore, the reactivity is high and the reaction rate is fast on the corners. As a result, the sharp surface of a high curvature easily formed holes, then the OH^- ions could continue to penetrate the interior of the cubes through the open holes, and further dissolution occurs inside the cubes since the outer part of the solid cube is more stable than the inner part. Subsequently, hollow cubes would be generated followed by the continuous release of $Zn(OH)_4^{2-}$ and $Sn(OH)_6^{2-}$ [Eq. (2)].[31]

C. Photo-absorption property

The absorption ability of materials can profoundly affect their photocatalytic activities. ZHS, as a ternary wide band gap semiconductor, can be excited to produce electron-hole pairs under 254 nm UV light irradiation.[20] Figure 3 shows the UV-vis absorption spectra of these as-prepared samples. These samples show a strong photo-absorption property in the UV light region. The absorption edges of the four samples were located at 270 nm (S4), 316 nm (S1), 386 nm (S2), and 380 nm (S3), respectively. Correspondingly, their band gaps can be determined to be 4.31 eV (S4), 3.92 eV (S1), 3.21 eV (S3), and 3.18 eV (S2). The S4 (hollow structure) has a wider band gap energy than other solid samples, which might be due to the blue shift caused by its nanosized cell wall (50–100 nm).

D. Surface areas and porestructure

The BET specific surface areas of the as-prepared samples, calculated from N_2 isotherms at 77 K, were 54.4 m^2/g(S4), 30.4 m^2/g(S3), 10.3 m^2/g(S2), and 5.7 m^2/g (S1), respectively.[32] The adsorption–desorption isotherm (Fig. 4) of the hollow ZHS sample shows gradual adsorption and desorption, exhibited the type IV isotherm, indicating that it has a mesoporous structure.[33] The average pore size of the hollow sample was 4.0 nm with 3.0 nm range distribution of the pore size.

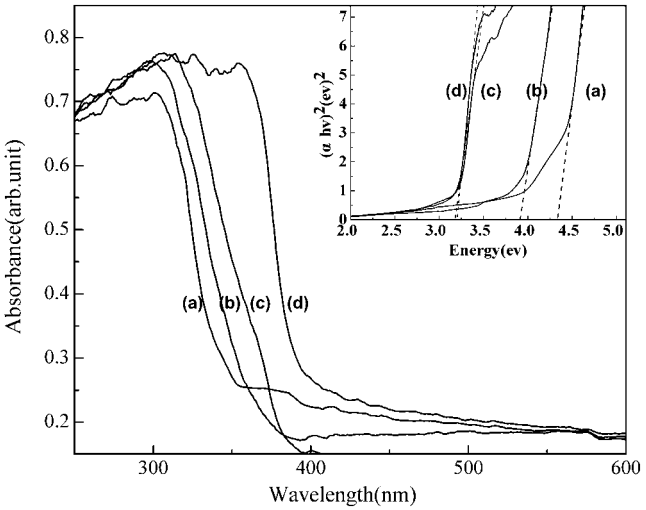


FIG. 3. The UV-vis absorption spectra and optical band gap energy (E_g) of (inset) as-prepared ZHS. (a) S4, (b) S1, (c) S2, and (d) S3.

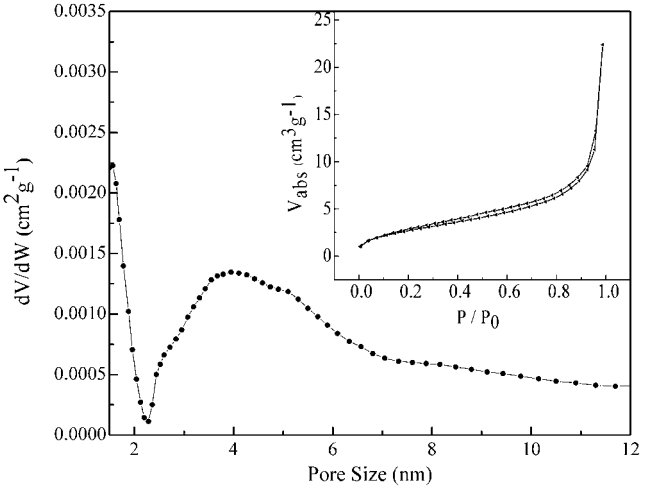


FIG. 4. The nitrogen adsorption–desorption isotherm (inset) and the pore size distribution plot for ZHS (S4).

https://doi.org/10.1557/jmr.2013.147 Published online by Cambridge University Press

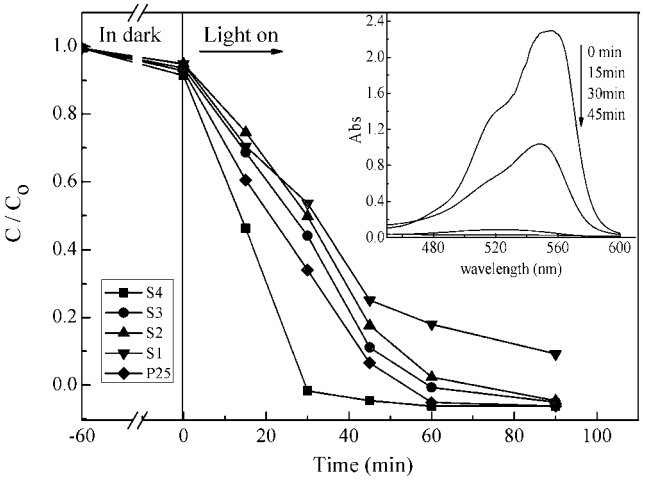


FIG. 5. Concentration percent of photocatalytic degradation of RhB as a function of irradiation time and time-dependent absorption spectral pattern of RhB in the existence of ZHS (S4) (inset).

E. Catalytic performance

Figure 5 shows the photocatalytic efficiency of different samples in RhB photodegradation in aqueous solution. The amount of TiO_2 is same as that of ZHS (0.5 g/L). As shown in Fig. 5, the photocatalytic activity of S4 (hollow structure) is much higher than that of other ZHS samples (solid structure). Actually, the photocatalytic activity is even higher than that of P25. Based on the results of characterizations, we think the strong activity might be mainly attributed to a synergy effect of its large BET surface area, wide band gap, and high crystallinity.[34]

In general, all photocatalytic activity is mainly influenced by three factors: (i) the adsorption ability of the reactants, (ii) the photo-absorption ability in the available light energy region, (iii) the separation and transporting rate of the photo-generated electrons and holes in catalyst.[35] With a larger surface area (54 m^2/g) than other three ZHS catalysts, S4 (hollow structure) would have stronger adsorption toward dye (RhB), which is beneficial for the reaction of dye and the active species generated on the surface, such as ·OH or O_2^-, etc. Meanwhile, it is widely accepted that the active species (·OH or O_2^-) are originated from the reaction of photoinduced electrons (e_{cb}^-) or holes (h_{vb}^+) with the absorbed O_2 or OH^-. The redox ability of the electrons and holes shows great effect on the reaction. The higher the oxidation ability of the holes is, the easier the ·OH species is generated. So is the relationship of the electron's reducibility and the formation of O_2^-. The band potential of ZHS and P25 was calculated based on the literature reported (Table I).[36,37] As shown in Table I, S4 exhibits the most negative conduction band (CB) potential and the most positive valence band (VB) potential due to its wide band gap (4.31 eV). It indicated that the photogenerated electrons and holes on S4 would have the stronger reducibility and oxidation ability than that on the other three ZHS samples. The photocatalytic reaction can be processed more smoothly. A higher photocatalytic activity is thus obtained on the S4 sample.

TABLE I. Absolute electronegativity, estimated band gap, energy levels of calculated CB edge, and VB at the point of zero charge for TiO_2 and $SnZn(OH)_6$.

Semiconductor oxides	Absolute electronegativity (X) (eV)	Calculated CB position (eV)	Calculated VB position (eV)	Estimated energy band gap, E_g (eV)
TiO_2	5.81	−0.29	2.91	3.20
ZHS(S1)	6.408	0.05	3.87	3.92
ZHS(S2)	6.408	0.32	3.50	3.18
ZHS(S3)	6.408	0.30	3.51	3.21
ZHS (S4)	6.408	−0.19	4.12	4.31

Actually, the difference in band potential can also be used to explain the different activities of S4 and P25 since they present the similar adsorption of RhB due to their close surface area. Although S4 and P25 exhibit a similar CB potential, the VB potential of S4 is more positive than that of P25 (see Fig. S3). The holes on S4 would exhibit stronger oxidation ability, which result in its higher photocatalytic activity.

In addition to the adsorption of dyes and the band potential, the separation and transporting rate of the photo generated electrons and holes in the catalyst also play an important role in the photocatalytic reactions. When the semiconductor $ZnSn(OH)_6$ was irradiated by light with energy larger than its band gap, electron/hole pairs would be generated. However, most of the electron–hole pairs would recombine the defect of the catalyst. Only a small part of them could migrate to the surface of the catalyst and react with the dyes. The defect density is a concept contrary to crystallinity. The S4 sample exhibits the highest crystallinity, which means that the sample contains the smallest amount of defect. Much more electrons and holes can be separated and can join the photocatalytic reaction, which would increase the photoactivity of S4. Lastly, it is considered that the special morphology of S4 might show some contributions on its high photoactivity. The hollow structure might improve the utilization of light since the incident light can be reflected in the hole. Under the same time of light irradiation, S4 sample can absorb most of light and generate most of electron–hole pairs, which is also beneficial for the photocatalytic reaction.

The stability of the as-prepared S4 sample (hollow structure) is also discussed in this paper. After 5 trials of recycle, shown in Fig. 6, no obvious deactivation was observed. The XRD patterns and SEM morphology of the fresh and used S4 sample also show no change (see Figs. S4 and S5), proving that the as-prepared ZHS (hollow structure) is very stable. Moreover, the raw materials for preparation of ZHS are very cheap and the preparation methods are quite simple and convenient, which all make ZHS more beneficial for further application.[34]

https://doi.org/10.1557/jmr.2013.147 Published online by Cambridge University Press

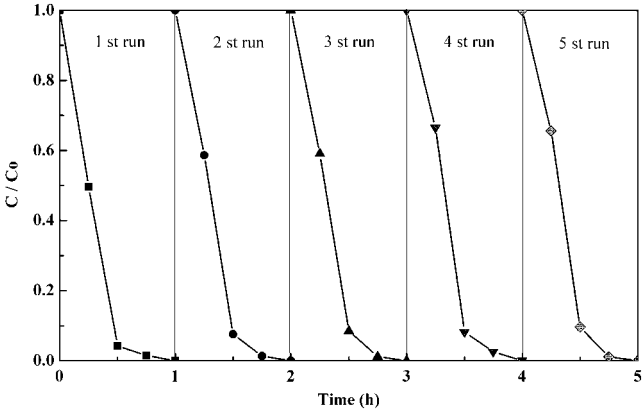


FIG. 6. Five recycles for the photodegradation of RhB with S4 (hollow structure).

IV. CONCLUSIONS

In summary, ZHS particles with different morphologies were synthesized by an alkali-assisted dissolution process at room temperature. The influence of ZHS photocatalytic activities with different morphologies was studied. This research obviously showed that the morphologies of ZHS, which strongly depended on the amount of solid NaOH, have great influence on their photocatalytic activities. The hollow structure ZHS, with a large BET surface area, wide band gap, and high crystallinity, exhibited the highest photocatalytic efficiency.

ACKNOWLEDGMENTS

This work was financially supported by the National Natural Science Foundation of China (Grant No. 21003109), the Applied Research Foundation of Public Welfare Technologies of Zhejiang Province (Grant No. 2012C37057), and the program for Zhejiang Leading Team of Science and Technology Innovation (Grant No. 2009R50020).

REFERENCES

1. X.W. Lou, L.A. Archer, and Z.C. Yang: Hollow micro-/nanostructures: Synthesis and applications. *Adv. Mater.* **20**, 3987 (2008).
2. H.G. Zhang, Q.S. Zhu, Y. Zhang, Y. Wang, L. Zhao, and B. Yu: One-pot synthesis and hierarchical assembly of hollow Cu_2O microspheres with nanocrystals-composed porous multishell and their gas-sensing properties. *Adv. Funct. Mater.* **17**, 2766 (2007).
3. Z. Yang, D.Q. Han, D.L. Ma, H. Liang, L. Liu, and Y.Z. Yang: Fabrication of monodisperse CeO_2 hollow spheres assembled by nano-octahedra. *Cryst. Growth Des.* **10**, 291 (2009).
4. W. Cheng, K.B. Tang, Z.P. Liu, J. Sheng, and Y.X. Qi: Template-free synthesis of monodisperse $Cu_2WO_4(OH)_2$ round and elliptical hollow spheres with a ligand-assisted dissolution process. *Chem. Commun.* **46**, 7185 (2009).
5. Y.R. Ma and L.M. Qi: Solution-phase synthesis of inorganic hollow structures by templating strategies. *J. Colloid Interface Sci.* **335**, 1 (2009).
6. H.G. Yu, J.G. Yu, S.W. Liu, and S. Mann: Template-free hydrothermal synthesis of CuO/Cu_2O composite hollow microspheres. *Chem. Mater.* **19**, 4327 (2007).
7. H. Jena, K.V.G. Kutty, and T.R.N. Kutty: Ionic transport and structural investigations on $MSn(OH)_6$(M = Ba, Ca, Mg, Co, Zn, Fe, Mn) hydroxide perovskites synthesized by wet sonochemical methods. *Mater. Chem. Phys.* **88**, 167 (2004).
8. A.N. Christensen, N.C. Broch, O. Heidenstam, and A. Nilsson: Hydrothermal investigation of the systems In_2O_3-H_2O-Na_2O and In_2O_3-D_2O-Na_2O. The crystal structure of rhombohedral In_2O_3 and of $In(OH)_3$. *Acta Chem. Scand.* **21**, 1046 (1967).
9. H.Q. Chiang, J.F. Wager, R.L. Hoffman, J. Jeong, and D.A. Keszler: High mobility transparent thin-film transistors with amorphous zinc tin oxide channel layer. *Appl. Phys. Lett.* **86**, 013503 (2005).
10. J.Z. Xu, C.Y. Zhang, H.Q. Qu, and C.M. Tian: Zinc hydroxystannate and zinc stannate as flame-retardant agents for flexible poly(vinyl chloride). *J. Appl. Polym. Sci.* **98**, 1469 (2005).
11. F. Andre, P.A. Cusack, A.W. Monk, and R. Seangprasertkij: The effect of zinc hydroxystannate and zinc stannate on the fire properties of polyester resins containing additive-type halogenated flame retardants. *Polym. Degrad. Stab.* **40**, 267 (1993).
12. P.R. Hornsby, P. Winter, and P.A. Cusack: Flame retardancy and smoke suppression of chlorosulphonated polyethylene containing inorganic tin compounds. *Polym. Degrad. Stab.* **44**, 177 (1994).
13. Z.Y. Yuan, F. Huang, J.T. Sun, and Y.H. Zhou: An amorphous nanosized tin-zinc composite oxide as a high capacity anode material for lithium ion batteries. *Chem. Lett.* **31**, 408 (2002).
14. A. Rong, X.P. Gao, G.R. Li, T.Y. Yan, H.Y. Zhu, J.Q. Qu, and D.Y. Song: Hydrothermal synthesis of Zn_2SnO_4 as anode materials for Li-ion battery. *J. Phys. Chem. B* **110**, 14754 (2006).
15. Y. Cao, D.Z. Jia, J. Zhou, and Y. Sun: Simple solid-state chemical synthesis of $ZnSnO_3$ nanocubes and their application as gas sensors. *Eur. J. Inorg. Chem.* **27**, 4105 (2009).
16. X.L. Fu, X.X. Wang, Z.X. Ding, D.Y.C. Leung, Z.Z. Zhang, J.L. Long, W.X. Zhang, Z.H. Zhao, and X.Z. Fu: Hydroxide $ZnSn(OH)_6$: A promising new photocatalyst for benzene degradation. *Appl. Catal., B* **91**, 67 (2009).
17. J.Q. Xu, Y.L. Liu, and X.S. Niu: Preparation and gas sensitivity of nanosized $ZnSnO_3$. *J. Chin. Ceram. Soc.* **30**, 321 (2002).
18. Z.G. Lu and Y.G. Tang: Two-step synthesis and ethanol sensing properties of Zn_2SnO_4-SnO_2 nanocomposites. *Mater. Chem. Phys.* **92**, 5 (2005).
19. C. Burda, X.B. Chen, R. Narayanan, and M.A. El-Sayed: Chemistry and properties of nanocrystals of different shapes. *Chem. Rev.* **105**, 1025 (2005).
20. Y.B. Chen, D.Z. Li, M. He, Y. Hu, H. Ruan, Y.M. Lin, J.H. Hu, Y. Zheng, and Y. Shao: High photocatalytic performance of zinc hydroxystannate toward benzene and methyl orange. *Appl. Catal., B* **113–114**, 134 (2012).
21. H. Fan, S.Y. Ai, and P. Ju: Room temperature synthesis of zinc hydroxystannate hollow core-shell microspheres and their hydrothermal growth of hollow core-shell polyhedral microcrystals. *Cryst. Eng. Commun.* **13**, 113 (2011).
22. Z. Qin, Y.H. Huang, Q.Y. Wang, J.J. Qi, X.J. Xing, and Y. Zhang: Controllable synthesis of well-dispersed and uniform-sized single crystalline zinc hydroxystannate nanocubes. *Cryst. Eng. Commun.* **12**, 4156 (2010).
23. L.L. Wang, K.B. Tang, Z.P. Liu, D.K. Wang, J. Sheng, and W. Cheng: Single-crystalline $ZnSn(OH)_6$ hollow cubes via self-templated synthesis at room temperature and their photocatalytic properties. *J. Mater. Chem.* **21**, 4352 (2011).
24. D. Kim, Y. Jeong, K. Song, S.K. Park, G.Z. Cao, and J. Moon: Inkjet-printed zinc tin oxide thin-film transistor. *Langmuir* **25**(18), 11149–11154 (2009).
25. X.L. Fu, D.Y.C. Leung, X.X. Wang, W.W. Xue, and X.Z. Fu: Photocatalytic reforming of ethanol to H_2 and CH_4 over $ZnSn(OH)_6$ nanocubes. *Int. J. Hydrogen Energy* **36**, 1524 (2011).

https://doi.org/10.1557/jmr.2013.147 Published online by Cambridge University Press

26. Y.J. Wang, Y.M. He, T.T. Li, J. Cai, M.F. Luo, and L. Zhao, Photocatalytic degradation of methylene blue on $CaBi_6O_{10}/Bi_2O_3$ composites under visible light. *Chem. Eng. J.* **189–190**, 473 (2012).
27. X.L. Fu, X.X. Wang, J.L. Long, Z.X. Ding, T.J. Yan, G.Y. Zhang, Z.Z. Zhang, H.X. Lin, and X.Z. Fu: Hydrothermal synthesis, characterization, and photocatalytic properties of Zn_2SnO_4. *J. Solid State Chem.* **182**, 517 (2009).
28. W. Fan, X. Song, and Y. Bu: Selected-control hydrothermal synthesis and formation mechanism of monazite- and zircon-type $LaVO_4$ nanocrystals. *J. Phys. Chem. B* **110**(46), 23247 (2006).
29. Z.L. Wang: Transmission electron microscopy of shape-controlled nanocrystals and their assemblies. *J. Phys. Chem. B* **104**, 1153 (2000).
30. J.Z. Yin, F. Gao, C.Z. Wei, and Q.Y. Lu: Controlled growth and applications of complex metal oxide $ZnSn(OH)_6$ polyhedra. *Inorg. Chem.* **51**, 10990 (2012).
31. T. Lehnen, D. Zopes, and S. Mathur: Phase-selective microwave synthesis and inkjet printing applications of Zn_2SnO_4 (ZTO) quantum dots. *J. Mater. Chem.* **22**, 17732 (2012).
32. Y.D. Hou, X.C. Wang, L. Wu, Z.X. Ding, and X.Z. Fu: Efficient decomposition of benzene over a β-Ga_2O_3 photocatalyst under ambient conditions. *Environ. Sci. Technol.* **40**, 5799 (2006).
33. S.J. Gregg and K.S.W. Sing: *Adsorption, Surface Area and Porosity* (Academic Press, London, 1997), p. 111.
34. Z.Y. Liu, D.D. Sun, P. Guo, and J.O. Leckie: One-step fabrication and high photocatalytic activity of porous TiO_2 hollow aggregates by using a low-temperature hydrothermal method without templates. *Chem. Eur. J.* **13**, 1851 (2007).
35. W.K. Chang, K.K. Rao, H.C. Kuo, J.F. Cai, and M.S. Wong: A novel core–shell like composite In_2O_3 & $CaIn_2O_4$ for efficient degradation of methylene blue by visible light. *Appl. Catal., A* **321**, 1 (2007).
36. Y.M. He, L.H. Zhao, Y.J. Wang, H.J. Lin, T.T. Li, X.T. Wu, and Y. Wu: Synthesis, characterization and photocatalytic performance of $VDyO_x$ composite under visible light irradiation. *Chem. Eng. J.* **169**, 50 (2011).
37. Y.M. He, Y. Wu, T.L. Sheng, and X.T. Wu: Photodegradation of acetone over V-Gd-O composite catalysts under visible light. *J. Hazard. Mater.* **180**, 675 (2010).

Supplementary Material

Supplementary materials can be viewed in this issue of the *Journal of Materials Research* by visiting http://journals.cambridge.org/jmr.

https://doi.org/10.1557/jmr.2013.147 Published online by Cambridge University Press